External surface phenomena in dealumination and desilication of large single crystals of ZSM-5 zeolite synthesized from a sustainable source

Deizi Peron, Vladimir Zholobenko, James H.S. de Melo, Mickael Capron, Nicolas Nuns, Michèle Oberson de Souza, Liliana Feris, Nilson Marcilio, Vitaly Ordomsky, Andrei Khodakov

May 13th, 2019

External surface phenomena in dealumination and desilication of large single crystals of ZSM-5 zeolite synthesized from a sustainable source

Deizi V. Peron[a,b], Vladimir L. Zholobenko[c], James H. S. de Melo[b], Mickael Capron[a], Nicolas Nuns[a], Michèle Oberson de Souza[b], Liliana A. Feris[b], Nilson R. Marcilio[b], Vitaly V. Ordomsky[a] and Andrei Y. Khodakov[a]*

[a]*Univ. Lille, CNRS, Centrale Lille, ENSCL, Univ. Artois, UMR 8181 – UCCS – Unité de Catalyse et Chimie du Solide, F-59000 Lille, France*

[b]*Universidade Federal do Rio Grande do Sul - UFRGS, Porto Alegre, RS 90040-040, Brazil*

[c]*School of Physical and Chemical Sciences, Keele University, Staffordshire, ST5 5BG, United Kingdom*

**andrei.khodakov@univ-lille.fr (Corresponding author)*

Abstract

Zeolite dealumination and desilication are common methods, which improve accessibility of the active sites located inside the zeolite crystallites and tune the zeolite acidity. The exact mechanism of these post-synthesis zeolite treatments remains under discussion. In this paper, a series of dealuminated and desilicated ZSM-5 zeolites are prepared using single or combined post-synthesis dealumination and desilication of large zeolite single crystals with oxalic acid and sodium hydroxide. The ZSM-5 zeolite has been synthetized using silica extracted from fly ash. Zeolite desilication results in the potholes, leaf-type structures and other clearly visible defects on the surface of zeolite crystallites, while the effect of dealumination is less pronounced. The low temperature nitrogen adsorption suggests the formation of mesopores in the zeolites formed by the voids between and in the irregular zeolite crystallites produced during post-synthesis treatments. ^{27}Al and ^{29}Si MAS NMR in combination with XRD data are indicative of only minor modifications of the bulk zeolite structure during dealumination and desilication. The total Brønsted acidity only slightly decreases and is not affected by the type of zeolite post-synthesis treatment. After desilication of large single crystals of ZSM-5, noticeable enhancement of the Brønsted acidity on the zeolite external surface has been detected by FTIR of absorbed collidine. The zeolites with higher acidity on the external surface have shown higher activity in the anisole acylation with hexanoic acid. A combination of characterization techniques suggests that the dealumination and desilication of the large crystals of ZSM-5 zeolite using post-synthesis treatments respectively with acid and alkali selectively starts at the zeolite external surface.

Keywords: mesoporous zeolite; ZSM-5; post-synthesis; external surface; acidity

1. Introduction

Zeolites are crystalline microporous aluminosilicates, which are widely used in adsorption, separation and catalysis. Zeolites are synthetized from silica and alumina sources usually in the presence of structure-directing agents, which are also called templates, under hydrothermal conditions. Synthesis of zeolites from fly ash has become increasingly attractive [1,2] in many countries, because of the challenges associated with coal production and fly ash disposal. In Brazil, ~4 million tons of coal ash are produced annually in the thermoelectric and industrial sectors [3–5]. The often irregular and uncontrolled deposition of this waste causes environmental problems, such as contamination of groundwater, soil and imbalance of ecological systems. Therefore, sustainable applications of fly ash are desirable to mitigate environmental pollution and health hazard. High silica content makes fly ash a suitable feedstock for the production of zeolite materials. The first step in fly ash utilization involves dissolution of the crystalline and amorphous phases of the ash in alkaline medium (NaOH or KOH) in order to make the Si and Al available for the formation of the zeolite framework during crystallization.

The benefits of zeolites for many industrial applications arise from their regular crystalline structure, high surface area, developed porosity, high stability, intrinsic acidity and an opportunity to introduce functionalities such as metal cations, metal clusters, organic complexes or enzymes. The acidity type, acid site amount, strength, and possible synergies with other zeolite active sites are extremely important for catalytic applications of zeolite-based materials. The small size of zeolite micropores can result in shape

selectivity effects [6] in catalytic reactions, when the size of the reaction products, intermediates or reagents can be limited by the size of zeolite micropores.

The small pore size of zeolites can also be a drawback, which may limit catalytic conversion of larger molecules over the active sites located inside the zeolite crystallites and which can lead to significant coke deposition [7] . Several techniques have been used in order to improve the accessibility of zeolite active sites located within the zeolite crystals. One of the most common approaches to increase the accessibility of active sites for reacting molecules is the design of hierarchical zeolites. In addition to regular microporous networks, hierarchical zeolites contain a significant mesoporous volume. Extensive mesoporous network of hierarchical zeolite can significantly facilitate the diffusion of reacting molecules and products. There have been two main approaches for obtaining hierarchical zeolites [8]. The first one is called the “bottom-up” or templating strategy, which can be divided into (i) soft templating that includes amphiphilic organosilanes, quaternary ammonium-form surfactants and more recently ionic liquids [9,10], (ii) hard templating with typically carbon materials such as carbon blacks, carbon nanotube, carbon nanofibers, polymers or resin; and (iii) indirect templating. In the indirect templating method, the zeolite hierarchical structure is produced by partial “zeolitisation” of the amorphous walls of mesoporous materials.

The alternative “top-down” strategy addresses post-synthesis chemical modification of zeolite crystals by treatment with steam, acid or basic agents. These treatments lead to the extraction of aluminum and silicon atoms and modification of the zeolite framework [11]. Both “bottom-up” and “top-down” strategies for the synthesis of hierarchical zeolites have their advantages and drawbacks. Though the “bottom-up” methods generally yield more ordered mesoporous zeolites, high cost of templates and methodological difficulties restrict large-scale applications of templating methods, in particular at the larger industrial

scale. Creating mesoporosity in microporous materials using the “top-down” method leads to less disordered mesoporous structures but at the same time, facilitates manufacturing larger quantities of hierarchical zeolites. The major challenge in the design of hierarchical zeolite using the “top-down“ method is to keep high zeolite crystallinity and micropores during generation of the mesopores.

The top-down post-synthesis zeolite modifications can involve dealumination and desilication [12]. Dealumination is a well-known post-synthesis method of removing aluminum from zeolite structure with the use of chemical agents or by hydrothermal treatment [13] . The goal of dealumination is to modify the Si/Al ratio in the zeolite framework and zeolite acidity, while the zeolite mesoporous structure can be affected to a variable degree depending on the treatment conditions. One of the major disadvantages of dealumination is possible blockage of the zeolite micropores by the weakly acidic extra-framework species. Though the presence of these extra-framework species and their interaction with Brønsted acid sites can enhance the catalytic performance of zeolites in some reactions [14,15], these species can also promote very significant carbon deposition, which would lead to fast catalyst deactivation [16].

The “desilication” method, which preferentially extracts silicon atoms from the zeolite framework, has been efficient for introducing additional mesopores, in particular, into high silica zeolites such as ZSM-5, Beta and mordenite. During desilication, the Al atoms, which were removed from the zeolite framework, can be subsequently reinserted into the tetrahedral positions of mesopore walls forming acidic hydroxyls. The extraction of silicon atoms from the framework is accompanied by partial breakdown of the zeolite structure generating additional porosity, mainly in the mesoporous range. Depending on the zeolite treatment conditions, dealumination or desilication may lead to significant changes in the acidic properties of the zeolite, such as the number and strength of

Brønsted and Lewis acid sites [17]. Dealumination and desilication can produce different effects on the zeolite smaller and larger crystals. A more significant amorphisation of the zeolite is expected, when small size zeolite crystals are subjected to post-synthesis treatments.

Dealumination and desilication could be used as complementary methods to control zeolite acidity, to create porosity and to improve the transport properties. On one hand, desilication leads to the abundant mesopore development, while on the other hand, dealumination removes aluminum-rich species, which typically exhibit weaker Brønsted acidity, and can result in extensive coke formation and pore blocking during catalytic reactions. A combination of desilication and dealumination could therefore represent an optimum strategy for the design of hierarchical zeolites with the best balanced mesoporosity, crystallinity and acidity. Sun *et al*. [18] showed that combined dealumination and desilication removed extra-framework aluminum, preserved intrinsic microporosity, improved the acid site accessibility and catalytic performances in cracking of heavy oils. This approach was also used by Feng [19] to obtain a hierarchical structure with a partial breakdown of the crystallites and high amounts of both Brønsted and Lewis acid sites. The synergetic effects of Brønsted and Lewis acid sites n a ZSM-5 catalyst facilitated n-heptane conversion, while "cleaner" micropores and newly created mesopores facilitated higher olefin selectivity and suppressed coke deposition. Dealumination and desilication were used by Xin *et al.* [20] to fine-tune the amounts of weak and strong acid sites in the zeolites. The acid strength had a major effect on the product distribution for ethanol conversion to ethylene and diethyl ether over ZSM-5 catalysts, and higher selectivity toward ethylene was associated with the increasing weak acidity observed on these post-treated catalysts.

The present paper explores the effect of combining dealumination and desilication treatments and their different sequences on the structure and acidity of the larger ZSM-5 zeolite crystals prepared from a sustainable source of silica such as coal fly ash. The structural characterization data are discussed alongside the catalytic performance of the zeolite material in anisole acylation with hexanoic acid. Acylation was used as a model reaction probing the zeolite acidity on the external surface of the crystallites and in the mesopores, which are developing during the zeolite post-synthesis treatments.

2. Materials and methods

2.1 Material preparation

The ZSM-5 zeolite was synthesized in our laboratories using fly ash as a silica source derived from the combustion of Candiota mineral coal (RS, Brazil). The silica was extracted by leaching the fly ash, which was generated during coal burning, using a hydrothermal process in the presence of an alkaline solution of sodium hydroxide, adapted from Cardoso *et al* [3]. **Figure 1** shows major steps involved in the extraction of silica from fly ash. In a typical preparation, 25 g of fly ash was suspended in 150 mL of an aqueous solution of NaOH in a 250-mL Schott bottles. Then, the flask containing the NaOH and ash mixture was placed in an oven at a given temperature, so that the silica leaching could occur.

After the leaching step, the suspension was subjected to vacuum filtration. Then, the pH of the filtrate was adjusted to 7.0 using HCl in order to precipitate the silica. The suspension was filtered again and the solid material, silica retained in the filter, was washed with 200 mL of distilled water and dried in an oven at 100 ºC for 12 h. In order to evaluate the influence of the temperature, time and molar concentration of NaOH solution on the coal ash silica extraction method and to define the best extraction

conditions, a rotational central composite design was used. Statistical analyses of the influence of the extraction parameters on the silica yield were performed with the software Statistica 8.0 (Stat Soft Inc., OK, USA), using the pure error that was calculated from the central point repetitions.

2.2.Zeolite synthesis

The zeolite synthesis was conducted in an autoclave at 190°C for 50 h in the presence of silica extracted from fly ash, aluminum sulfate, sodium sulfate, sodium hydroxide and N-butylamine (SiO_2:0.02$Al_2(SO_4)_3$:0.3$C_4H_{11}N$:0.24NaOH:0.16Na_2SO_4:40H_2O). After the hydrothermal synthesis, the zeolite sample was washed, dried and calcined to remove the organic template, and then converted into the H-form *via* ion exchange with ammonium nitrate followed by calcination at 450°C. The as-prepared ZSM-5 zeolite (with Si/Al ratio of 17 as determined by XRF) was then subjected to either dealumination or desilication, or both. The desilication treatment was performed in aqueous media: 1 g of the parent zeolite was added to 30 mL of solution of 0.2 M NaOH for 30 min at 65 ºC, as reported by Groen [21]. After the alkaline treatment, the sample was washed, dried and calcined, then converted into H-form *via* ion exchange with ammonium nitrate followed by calcination at 450°C. The desilicated sample is referred to **DeSi**. Dealumination treatment of the parent zeolite was carried out in 90 mL of 0.1 M aqueous solution of oxalic acid for 3 h at 80 ºC following the procedure described by Bonilla *et al* [22]. After the acid treatment, the sample was washed, dried and calcined at 450ºC, and then converted into the H-form *via* ion exchange with ammonium nitrate followed by calcination at 450°C. This sample was labelled as **DeAl.** After the primary desilication or dealumination, a second treatment was performed: the desilicated zeolite was dealuminated and the dealuminated zeolite was subjected to desilication. The sample with the desilication as

the primary treatment was referred to **DeSiDeAl**, while the sample with the primary dealumination treatment was labelled as **DeAlDeSi.**

2.3 Catalyst characterization

The sample chemical composition was determined by X-ray fluorescence (XRF) using a M4 TORNADO (Bruker) spectrometer. The instrument was equipped with 2 anodes, a rhodium X-ray tube (50 kV/600 mA, 30 W) and a tungsten X-Ray tube (50 kV/700 mA, 35 W), and a Silicon-Drift-Detector Si(Li) (<145 eV resolution at 100000 cps (Mn Kα) with a Peltier cooling to 253°C). For sample characterization, the rhodium X-rays with a poly-capillary lens enabling excitation of an area of 200 µm were used. The measurements were conducted under vacuum (20 mbar). Quantitative analysis was performed using fundamental parameters (standardless).

The BET apparent surface area, pore volume, and average pore diameter were determined by low-temperature nitrogen adsorption using a Micromeritics ASAP 2000 automated system. The apparent surface areas of the catalysts was calculated using the BET model for the P/P_o relative nitrogen pressure <0.04. The samples were degassed under vacuum at <10 µmHg at 300°C for 4 h before N_2 physisorption. The total pore volume (TPV) was calculated from the amount of vapor adsorbed at a relative pressure close to unity by assuming that the pores are completely filled with the condensate in the liquid state. The catalyst external surface area and micropore volume were calculated using the deBoer t-plot method.

The samples were characterized by X-ray diffraction (XRD) using a D8 Advance diffractometer equipped with an energy dispersive detector and a monochromatic CuK_α radiation source. The samples were analyzed using a step of 0.02° with an acquisition time of 0.5 s.

The electron micrographs were obtained by FEI-Quanta 200 scanning electron microscope (SEM) equipped with a field emission gun. Comparative characterization of the Brønsted and Lewis acid sites (BAS and LAS) in zeolites was carried out using transmittance FTIR measurements in the 6000-900 cm^{-1} spectral range utilizing pyridine (Py) and collidine (2, 4, 6-trimethyl pyridine) adsorption. Py was used for measuring the total number of BAS and LAS in the zeolites, while adsorption of collidine was used for evaluation of the number of acid sites on the zeolite external surface and mesopores as the relatively large size of collidine (7.9 Å) prevents its access to acid sites in the ZSM-5 micropores. FTIR transmittance measurements were performed at ~60°C using catalyst self-supported disks activated at 450°C for 5 h in vacuum (with the temperature ramp of 1°C/min). FTIR spectra were collected using a Thermo iS10 spectrometer at a 4 cm^{-1} resolution (0.96 cm^{-1} data spacing). The spectra were analyzed using specialized Thermo software, Omnic. An excess of Py or collidine was admitted into the transmittance cell at 150°C, in a stepwise manner until no changes were observed in the spectra. The saturated sample was then evacuated for 20 min at 150°C to remove physically adsorbed molecules. To quantify the number of acid sites from the area of the corresponding IR peaks of adsorbed Py, the following values of the molar absorption coefficients were used: ε (B, ZSM-5)=1.08 and ε (B, BEA)=1.16 cm μmol^{-1} for Brønsted acid sites (peak at ~1546 cm^{-1}) and ε(L)=1.71 cm μmol^{-1} for Lewis acid sites (peaks at ~1455-1445 cm^{-1}). The ε (B, collidine)=10.1 cm μmol^{-1} was used for calculating the concentration of BAS on the zeolite external surface from the spectra of adsorbed collidine [23,24]. Because of the steric hindrances introduced by methyl groups, collidine (2,4,6-trimethyl-pyridine) did not interact with the Lewis acid sites.

The ^{29}Si MAS NMR measurements were carried out utilizing a Bruker AVANCE spectrometer with the ^{29}Si Larmor frequency of 79.49 MHz and a 7 mm MAS rotor

spinning at 5 kHz and using a $\pi/2$ pulse length of 4.75 µs. For the ^{27}Al resonance measurement, the spectrometer used was Bruker AVANCE NEO operating at ^{27}Al Larmor frequency of 208.48 MHz with a 3.2 mm MAS rotor spinning at 22 kHz and using a $\pi/12$ pulse length to ensure a quantitative excitation of the central transitions [25]. The analysis of the spectra was performed using DM Fit software [26]. The ^{27}Al and ^{29}Si chemical shifts were referenced relative to 1 M $Al(NO_3)_3$ aqueous solution and $Si(CH_3)_4$, respectively.

ToF-SIMS analyses were carried out to characterize the aluminum and silicon contents at the surface of the samples. For this a ToF-SIMS machine has been used (IONTOF GmbH Germany) equipped with a bismuth liquid metal ion gun (LMIG). The powder samples have been tableted before the analysis in order to reduce surface roughness and then improve mass resolution. Pulsed Bi_3^+ (25keV -0.25 pA) was used for analysis in positive mode over an area of 500 x 500 μm^2. With these experimental conditions, secondary ions detected over time of flight analyzer were collected from the first 3 nm of our samples. In order to compensate charges induced by primary ion beam, a low energy (20 eV) pulsed electron flood gun has been used. Positive spectra obtained had a mass resolution of $\approx$ 3500 at m/z = 28 for silicon. It was possible to detect and identify easily many molecular secondary ions related to Si. This was not the case for aluminum, since Al^+ was the only secondary ions clearly detected on each samples.

2.4. Catalytic tests

The activity of all catalysts was evaluated in the acylation reaction between anisole and hexanoic acid according to the following protocol. The catalyst (20 mg) was added to a mixture of anisole (2 g) and hexanoic acid (0.3 g) in a reflux reactor system (under

stirring) and heated at 180 °C for 2 h. The products were analyzed using gas-chromatography.

3. Results and Discussion

3.1. Optimization of silica extraction from fly ash

First, the procedure for silica extraction from fly ash was optimized. The extraction temperature, extraction time and molar concentration of NaOH solution were process variables evaluated in this study (**Table S1, Supplementary Information (SI)**). The analyzed response variable was the mass yield of extracted silica. The influence of the NaOH concentration, the extraction time and temperature on the mass of the extracted silica is displayed in **Figures S1, S2 and S3 (SI)**. The increase in time and the NaOH concentration favor silica extraction, whereas the effect of the extraction temperature is more complicated. The extraction yield reaches the maximum value at the temperatures between 100 and 120 ºC. Based on the data analysis using a regression model, the following optimum conditions were selected in order to boost the yield of silica: temperature of 100 ºC, time of 72 h and NaOH concentration of 4 mol L^{-1}. Finally, the silica yield of 89.09 % was obtained. The XRD patterns of the extracted silica exhibiting a broad hallo attributed to the amorphous phase are displayed in **Figure S4, SI.** The silica extracted from fly ash was amorphous. The elemental composition of the silica extracted from fly ash was evaluated using XRF (**Table S2, SI**). In addition to Si and O, the sample contained small amounts of aluminum (1.10 wt.%), sodium (2.97 wt. %) and potassium (0.48 wt.%).

3.2. Characterization of dealuminated and desilicated ZSM-5 zeolites

Figure 2 displays XRD patterns of the parent ZSM-5, dealuminated and desilicated zeolites. The intense XRD peaks characteristic of the MFI structure are observed in all samples. The sharp, well defined XRD peaks indicate the presence of relatively large zeolite crystallites. The dealumination and desilication treatments of the ZSM-5 catalyst do not result in any significant changes in the intensity, width and position of the XRD peaks, and no halo peaks, which can be attributed to the amorphous phase, have been detected. Overall, no noticeable decrease in the crystallinity or in the size of the crystalline domains of the zeolite catalyst has been observed after the post-synthesis treatments.

The SEM images of the parent zeolite, dealuminated and desilicated samples are shown in **Figure 3**. The parent zeolite contains cubic and prismatic crystals characteristic of the ZSM-5 structure with the relatively large average size of 5-7 μm (**Figure 3a**). Desilication results in appearance of clearly visible potholes and cracks on the surface of the single ZSM-5 crystals, while their overall morphology remains almost intact (**DeSi** sample**, Figure 3b**). Interestingly, the formation of potholes and cracks is less pronounced with the dealuminated (**DeA**l) sample (**Figure 3c**). Zeolite treatment using combined dealumination and desilication leads to further noticeable changes: irregular shape of zeolite crystallites and the formation of leaf-type structure (**DeAlDeSi** and **DeSiDeAl** samples, **Figure 3d and e**).

Table 1 shows the chemical composition measured from XRF analysis and textural properties of the dealuminated and desilicated zeolites obtained from nitrogen adsorption-desorption isotherms. The overall Si/Al ratio is only slightly affected by dealumination and desilication. The nitrogen adsorption–desorption isotherms obtained for the studied zeolites are shown in **Figure 4**. The parent ZSM-5 sample displays a type I isotherm,

which exhibits a sharp uptake at low relative pressure followed by a plateau with a hardly visible hysteresis at $P/P_0>0.5$. This type of isotherm is usually observed for microporous materials with negligible textural mesoporosity generated by aggregation of zeolite crystallites. The dealumination treatment does not significantly affect the shape of the nitrogen isotherm (**DeAl, Figure 4a**), indicating that the oxalic acid treatment does not create additional mesopores in the zeolite. In contrast to dealumination, zeolite desilication results in noticeable changes in the shape of the adsorption isotherm (**DeSi, Figure 4b**), which presents a combination of type I and type IV isotherms showing a significant N_2 uptake at low relative pressure and a hysteresis loop at high relative pressure ($P/P_0>0.7$). This can be interpreted in terms of creating a new type of mesopores with relatively large pore sizes, which can correspond to the appearance of mesoporosity inside the zeolite crystallites or can arise from creating voids between and on the external surface of zeolites crystallites, whose shape was modified by the treatment in alkaline media. The nitrogen adsorption data are consistent with the SEM images, which clearly show the formation of potholes and cracks following desilication in the **DeSi** sample (**Figure 3b**). Subsequent dealumination does not affect the shape of isotherms (**Figure 4b**), while desilication of the dealuminated sample (**Figure 4a**) yields an additional hysteresis loop at $P/P_0>0.7$, which corresponds to the emergence of new mesopores or voids between and on the external surface of the zeolite crystallites. Note that the BET surface area is only slightly affected by the dealumination and desilication processes (**Table 1**).The BJH mesopore distribution curves are shown in **Figure S5, SI**. They show appearance of a peak corresponding to the pore radius from 30 to 60 Å corresponding to the mesopores created by the zeolite post-treatments. Interestingly, the intensity of this peak is lower and very small for the dealuminated **DeAl** zeolite. Desilication leads to a noticeable increase in the intensity of this peak. The higher intensity is attained for

DeSiDeAl sample whose preparation involved primary desilication. These results indicate that the desilication is the main process responsible for the introduction of mesoporosity to the post-treated zeolite.

The ^{27}Al MAS-NMR and ^{29}Si MAS-NMR spectra of the studied ZSM-5 zeolites displayed in **Figure 5.** The relative intensities of ^{27}Al MAS-NMR peaks summarized in **Table 2** indicate the presence of mostly tetrahedrally coordinated framework Al atoms. Indeed, the spectra show strong resonances with an isotropic chemical shift equal to 55.5 ppm, which is assigned to the four-fold coordinated Al atoms [27–29]. There is also a peak around 0 ppm representing approximately 10% of the aluminum atoms, which is assigned to the six-fold coordinated extra-framework Al species. Its intensity is higher for the zeolites subjected to combined dealumination and desilication. In addition to these peaks, NMR spectrum of the parent ZSM-5 shows a peak at 28.0 ppm assigned to penta-coordinated aluminum atoms [27]. The penta-coordinated Al species detected by ^{27}Al MAS-NMR correspond to the Al atoms partially removed from the zeolite framework. These species are present in the parent ZSM-5 zeolite. These labile species can easily change their coordination during dealumination or desilication, for instance they can be fully removed from or reinserted into the zeolite framework depending on the post-synthesis modification conditions.

The ^{29}Si MAS NMR spectra of the studied zeolites (**Figure 5b**) exhibit resonances at -106.2, -111.9 and -115.3 ppm which are characteristic of tetrahedral Si in ZSM-5 zeolites that are surrounded by 3 Si and 1 A1 or by 4 Si tetrahedra, (Q_4(1Al)) or (Q_4(0Al)) [30,31]. An example of the ^{29}Si MAS NMR spectrum deconvolution is given in **Figure S6, SI** and the relative intensities of the individual peaks are summarized in **Table 3**. The most prevalent type of SiO_4 tetrahedra is Q_4. Dealumination and desilication only slightly influence the relative intensity of ^{29}Si MAS NMR peaks. The Si/Al ratio calculated

according to Kilnowki *et al* [32] (Si/Al=19-21) is slightly higher than the value obtained from the XRF analysis (Si/Al=14-17), confirming the presence of some extra-framework aluminum species. Thus, the NMR results suggest a relatively small effect of dealumination and desilication treatments on the bulk structure of the large ZSM-5 zeolite crystals.

The acidity of the zeolites was evaluated using pyridine (Py) adsorption monitored by FTIR spectroscopy. Following Py adsorption, the zeolite spectra (**Figure 6)** exhibit characteristic bands at ~1545 and 1456 cm^{-1} attributed respectively to the pyridinium ion (PyH^+) formed on BAS and to the Py molecules coordinated to LAS. Py adsorbed on both LAS and BAS also displays a band at ~1490 cm^{-1}. **Table 4** shows the concentration of BAS and LAS calculated from the intensity of the FTIR bands at ~1545 and 1456 cm^{-1}. The amount of BAS (Py-BAS complexes) decreases in all zeolites after dealumination or desilication. Interestingly, combined treatments of the zeolite using dealumination or desilication (**DeAlDeSi** and **DeSiDeAl** samples) do not result in additional modification of the zeolite acidity. At the same time, the concentration of LAS (Py-LAS complexes) shows little change after the post-synthesis zeolite treatments.

Collidine adsorption over the zeolites gives rise to the band at ~1634 cm^{-1} with a shoulder at ~1649 cm^{-1} resulting from the interaction with BAS [33,34]; two low intensity bands at 1619 cm^{-1} and 1575 cm^{-1} are assigned to the probe adsorbed on Si-OH groups. The concentration of BAS measured from FTIR spectra of adsorbed collidine is shown in **Table 4**. Interestingly, zeolite desilication leads to a noticeable increase in the concentration of BAS on the external surface of the zeolites and in mesopores, while dealumination does not. This is also consistent with the appearance of defects on the surface of ZSM-5 crystallites after desilication observed by other techniques. Thus, the initial desilication noticeably improves access to the zeolite acid sites, probably, by

creating additional mesopores near the external surface of the large ZSM-5 crystals. In contrast, initial dealumination, even if it is producing additional mesopores near the external surface, seems to remove Al species and associated acid sites. It should be noted, that the number of accessible "external" acid sites, generated as the result of any treatment, is rather small.

The surface composition of the zeolite crystals was also investigated using ToF-SIMS. The intensities of the identified Al- and Si-containing fragments are shown in **Table S3, SI**. The variation of the intensities of Al^+ and Si^+ fragments provides qualitative information about the chemical composition of the zeolite external surface. As expected, the zeolite dealumination results in a major decrease in the ratio of intensities of Al^+ to Si^+ fragments from 0.43 in **ZSM-5** to 0.11 in **DeAl**. This corresponds to the decrease in Al concentration on the zeolite external surface. Desilication results in a less significant decrease in the Al^+/Si^+ intensity ratio (from 0.43 in **ZSM-5** to 0.26 in **DeSi**). Subsequent dealumination of the desilicated **DeSi** sample leads to a further decrease in the Al concentration, while some increase in the Al^+/Si^+ intensity ratio was observed after subsequent desilication of the **DeAl** sample. The Al^+/Si^+ intensity ratio drops from 0.23 to 0.13 in **DeSiDeAl**. Note that the variation of the Al^+/Si^+ intensity ratio on the zeolite external surface observed by ToF-SIMS does not correlate with the Brønsted acidity of the zeolite external surface measured from the FTIR spectra of adsorbed collidine. This is indicative of the presence of significant amounts of extraframework aluminum species on the zeolite external surface, which do not contribute to the Brønsted acidity.

Our results demonstrate that dealumination and desilication of the larger ZSM-5 zeolite crystals principally modify the external surface of the zeolites, while the zeolite volume is affected to a much lesser extent by these treatments. Indeed, the XRD data (**Figure 2**) suggest that the post synthesis treatments of the large ZSM-5 zeolite crystals do not

significantly affect the zeolite bulk structure. The intensities of XRD peaks are almost unaltered by dealumination, desilication or combined treatments. The concentration of acid sites inside the zeolite crystallites measured by Py adsorption slightly decreases after the dealumination, desilication or combined treatments (**Table 4**). Interestingly, the amount of BAS and LAS is almost the same in the dealuminated and desilicated zeolites. Both ^{27}Al and ^{29}Si MAS NMR show a minor effect of dealumination and desilication conducted sequentially or separately on the coordination of aluminium or silicon atoms in the zeolites. ^{27}Al MAS NMR (**Table 2**) shows little effects of different treatments on the amount of octahedrally coordinated extra-framework aluminum species. ^{29}Si MAS NMR (**Table 3**) shows only very slight effect of the post synthesis treatment on the local environment of silicon species. The Si/Al ratios measured by both XRF and ^{29}Si MAS NMR in the parent zeolite and in all dealuminated and desilicated samples are not affected by the treatments. All these data suggest very small effect of dealumination, desilication and combined treatments on the zeolite bulk structure.

It is important to note that the surface of the zeolite crystallites is affected to a much larger extent by the post-synthesis treatments. The SEM images (**Figure 3**) show a significant influence of desilication on the shape of the zeolites crystallites. Unlike dealumination, the zeolite desilication results in the formation of potholes, cracks and even leaf-type structures on the external surface of the zeolites. The modification of the ZSM-5 zeolite crystallites is even more significant in the samples subjected to a combination of desilication and dealumination. The SEM results are consistent with nitrogen adsorption data. Interestingly, it is mostly desilication that results in the appearance of additional large mesopores. These mesopores are probably created by the voids between and on the external surface of the irregular zeolite crystallites produced during the desilication. The acidity of the external surface of the zeolites has been evaluated using the FTIR spectra

of adsorbed collidine demonstrating the emergence of BAS on the external surface on the desilicated zeolite sample, which persist even after additional dealumination treatment. Our results strongly suggest that dealumination using oxalic acid and desilication with sodium hydroxide start at the external surface of the large ZSM-5 zeolite crystals. It should be noted that a prolonged treatment under more severe dealumination or desilication conditions can lead to the alternation of the bulk zeolite structure.

Acylation of anisole with hexanoic acid has provided additional information about the acidity of the zeolite external surface and reactivity of the zeolite acid sites in the dealuminated and desilicated zeolites (**Figure 7**). The large size of the reacting molecules suggests that this reaction occurs on the external surface of the zeolite. The selectivity to ortho-isomer was higher than 90% in all experiments and only traces of para- and meta-isomers have been detected. No correlation has been found between the anisole conversion and total amount of BAS in the zeolite as measured by Py adsorption (**Figure 8a**), confirming that the reaction does indeed take place on the zeolite external surface. The anisole conversion as a function of the Brønsted acidity on the external surface of the large zeolite crystals (as measured by collidine adsorption) is shown in **Figure 8b**. Higher anisole conversions are observed over the samples with a higher concentration of BAS on the external surface of the ZSM-5 crystallites, which is more easily achieved by the zeolite desilication. It is generally accepted that for high silica zeolites, such as ZSM-5 with Si/Al ratio above ~10, the "intrinsic" strength of their Brønsted acid sites does not change with a further increase in the Si/Al ratio, e.g. caused by dealumination. There is also no indication that the Brønsted acid sites on the external surface of zeolite crystals have a different strength as compared to those in the micropores of the same zeolite.

Conclusion

A combination of characterization techniques has provided important new insights into the phenomena occurring in the larger crystals of the ZSM-5 zeolite during dealumination with oxalic acid and desilication with sodium hydroxide. Both desilication and dealumination start at the external surface of the larger ZSM-5 zeolite crystals. Desilication and, to a lesser extent, dealumination result in the appearance of potholes and cracks on the external surface of larger ZSM-5 crystallites. These defects on the zeolite external surface and voids between and on the external surface of the irregular ZSM-5 crystals produced during the dealumination and desilication contribute to the development of zeolite mesoporosity. XRD, ^{27}Al and ^{29}Si MAS NMR do not show any noticeable modification of the zeolite bulk structure after the dealumination and desilication treatments. Zeolite desilication leads to the appearance of additional Brønsted acidity on the external surface of ZSM-5 zeolites, which contributes to a higher rate of anisole acylation with hexanoic acid over these systems.

Acknowledgement

The authors are grateful to Laurence Burylo, Bertrand Revel and Joelle Thuriot for help with XRD, NMR and XRF measurements. The authors thank International Cooperation Program CAPES/COFECUB Foundation funded by CAPES – Brazilian Federal Agency for Support and Evaluation of Graduate Education within the Ministry of Education of Brazil for providing a PhD stipend and financial support for this work. The Chevreul Institute (FR 2638), Ministère de l'Enseignement Supérieur, de la Recherche et de l'Innovation, Hauts-de-France Region and FEDER are acknowledged for supporting and partially funding this work. The authors acknowledge financial support of the French

National Research Agency (DirectSynBioFuel project, Ref. ANR-15-CE06-0004 and NANO4-FUT, Ref. ANR-16-CE06-0013).

References

[1] X. Querol, N. Moreno, J.C. Umana, A. Alastuey, E. Hernandez, A. Lopez-Soler, F. Plana, Synthesis of zeolites from coal fly ash: an overview, Int. J. Coal Geol. 50 (2002) 413–423. doi:10.1017/CBO9781107415324.004.

[2] T. V. Ojumu, P.W. Du Plessis, L.F. Petrik, Synthesis of zeolite A from coal fly ash using ultrasonic treatment – A replacement for fusion step, Ultrason. Sonochem. 31 (2016) 342–349. doi:10.1016/j.ultsonch.2016.01.016.

[3] A.M. Cardoso, M.B. Horn, L.S. Ferret, C.M.N. Azevedo, M. Pires, Integrated synthesis of zeolites 4A and Na-P1 using coal fly ash for application in the formulation of detergents and swine wastewater treatment, J. Hazard. Mater. 287 (2015) 69–77. doi:10.1016/j.jhazmat.2015.01.042.

[4] J.D.C. Izidoro, D.A. Fungaro, F.S. Dos Santos, S. Wang, Characteristics of Brazilian coal fly ashes and their synthesized zeolites, Fuel Process. Technol. 97 (2012) 38–44. doi:10.1016/j.fuproc.2012.01.009.

[5] L. Bieseki, F.G. Penha, S.B.C. Pergher, Zeolite A synthesis employing a brazilian coal ash as the silicon and aluminum source and its applications in adsorption and pigment formulation, Mater. Res. 16 (2012) 38–43. doi:10.1590/S1516-14392012005000144.

[6] B. Smit, T.L.M. Maesen, Towards a molecular understanding of shape selectivity, Nature. 451 (2008) 671–678. doi:10.1038/nature06552.

[7] J.L. Atwood, J.W. Steed, eds., Encyclopedia of Supramolecular Chemistry, CRC Press, 2004. doi:10.1081/E-ESMC.

[8] J. Li, M. Liu, X. Guo, S. Zeng, S. Xu, Y. Wei, Z. Liu, C. Song, Influence of Al Coordinates on Hierarchical Structure and T Atoms Redistribution during Base Leaching of ZSM-5, Ind. Eng. Chem. Res. (2018) acs.iecr.8b03539.

doi:10.1021/acs.iecr.8b03539.

[9] A. Sachse, C. Wuttke, E. Lissner, M. Oberson de Souza, Ordered Mesoporous ZSM-5 Employing an Imidazolium-Based Ionic Liquid, Chem. - A Eur. J. 20 (2014) 14996–14999. doi:10.1002/chem.201404568.

[10] A. Sachse, C. Wuttke, U. Díaz, M.O. de Souza, Mesoporous Y zeolite through ionic liquid based surfactant templating, Microporous Mesoporous Mater. 217 (2015) 81–86. doi:10.1016/j.micromeso.2015.05.049.

[11] A. Feliczak-Guzik, Hierarchical zeolites: Synthesis and catalytic properties, Microporous Mesoporous Mater. 259 (2018) 33–45. doi:10.1016/j.micromeso.2017.09.030.

[12] M.C. Silaghi, C. Chizallet, P. Raybaud, Challenges on molecular aspects of dealumination and desilication of zeolites, Microporous Mesoporous Mater. 191 (2014) 82–96. doi:10.1016/j.micromeso.2014.02.040.

[13] Y. Wei, T.E. Parmentier, K.P. de Jong, J. Zečević, Tailoring and visualizing the pore architecture of hierarchical zeolites, Chem. Soc. Rev. 44 (2015) 7234–7261. doi:10.1039/C5CS00155B.

[14] S. Schallmoser, T. Ikuno, M.F. Wagenhofer, R. Kolvenbach, G.L. Haller, M. Sanchez-Sanchez, J.A. Lercher, Impact of the local environment of Brønsted acid sites in ZSM-5 on the catalytic activity in n-pentane cracking, J. Catal. 316 (2014) 93–102. doi:10.1016/j.jcat.2014.05.004.

[15] S. Li, A. Zheng, Y. Su, H. Zhang, L. Chen, J. Yang, C. Ye, F. Deng, Brønsted/Lewis Acid Synergy in Dealuminated HY Zeolite: A Combined Solid-State NMR and Theoretical Calculation Study, J. Am. Chem. Soc. 129 (2007) 11161–11171. doi:10.1021/ja072767y.

[16] M. Hartmann, A.G. Machoke, W. Schwieger, Catalytic test reactions for the

evaluation of hierarchical zeolites, Chem. Soc. Rev. 45 (2016) 3313–3330. doi:10.1039/C5CS00935A.

[17] C.S. Triantafillidis, A.G. Vlessidis, N.P. Evmiridis, Dealuminated H−Y Zeolites: Influence of the Degree and the Type of Dealumination Method on the Structural and Acidic Characteristics of H−Y Zeolites, Ind. Eng. Chem. Res. 39 (2000) 307–319. doi:10.1021/ie990568k.

[18] H. Sun, P. Peng, Y. Wang, C. Li, F. Subhan, P. Bai, W. Xing, Z. Zhang, Z. Liu, Z. Yan, Preparation, scale-up and application of meso-ZSM-5 zeolite by sequential desilication–dealumination, J. Porous Mater. 24 (2017) 1513–1525. doi:10.1007/s10934-017-0391-4.

[19] R. Feng, X. Yan, X. Hu, Y. Wang, Z. Li, K. Hou, J. Lin, Hierarchical ZSM-5 zeolite designed by combining desilication and dealumination with related study of n-heptane cracking performance, J. Porous Mater. 25 (2018) 1743–1756. doi:10.1007/s10934-018-0587-2.

[20] H. Xin, X. Li, Y. Fang, X. Yi, W. Hu, Y. Chu, F. Zhang, A. Zheng, H. Zhang, X. Li, Catalytic dehydration of ethanol over post-treated ZSM-5 zeolites, J. Catal. 312 (2014) 204–215. doi:10.1016/j.jcat.2014.02.003.

[21] J.C. Groen, T. Bach, U. Ziese, A.M. Paulaime-Van Donk, K.P. De Jong, J.A. Moulijn, J. Pérez-Ramírez, Creation of hollow zeolite architectures by controlled desilication of A1-zoned ZSM-5 crystals, J. Am. Chem. Soc. 127 (2005) 10792–10793. doi:10.1021/ja052592x.

[22] A. Bonilla, D. Baudouin, J. Pérez-Ramírez, Desilication of ferrierite zeolite for porosity generation and improved effectiveness in polyethylene pyrolysis, J. Catal. 265 (2009) 170–180. doi:10.1016/j.jcat.2009.04.022.

[23] N.S. Nesterenko, F. Thibault-Starzyk, V. Montouilliout, V. V. Yushchenko, C.

Fernandez, J.-P. Gilson, F. Fajula, I.I. Ivanova, The use of the consecutive adsorption of pyridine bases and carbon monoxide in the IR spectroscopic study of the accessibility of acid sites in microporous/mesoporous materials, Kinet. Catal. 47 (2006) 40–48. doi:10.1134/S0023158406010071.

[24] T. Onfroy, G. Clet, M. Houalla, Quantitative IR characterization of the acidity of various oxide catalysts, Microporous Mesoporous Mater. 82 (2005) 99–104. doi:10.1016/j.micromeso.2005.02.020.

[25] A. Samoson, E. Lippmaa, Excitation phenomena and line intensities in high-resolution NMR powder spectra of half-integer quadrupolar nuclei, Phys. Rev. B. 28 (1983) 6567–6570. doi:10.1103/PhysRevB.28.6567.

[26] D. Massiot, F. Fayon, M. Capron, I. King, S. Le Calvé, B. Alonso, J.-O. Durand, B. Bujoli, Z. Gan, G. Hoatson, Modelling one- and two-dimensional solid-state NMR spectra, Magn. Reson. Chem. 40 (2002) 70–76. doi:10.1002/mrc.984.

[27] J. Klinowski, Applications of solid-state NMR for the study of molecular sieves, 283 (1993).

[28] M. Haouas, F. Taulelle, C. Martineau, Recent advances in application of 27Al NMR spectroscopy to materials science, Prog. Nucl. Magn. Reson. Spectrosc. 94–95 (2016) 11–36. doi:10.1016/j.pnmrs.2016.01.003.

[29] P. Sazama, E. Tabor, P. Klein, B. Wichterlova, S. Sklenak, L. Mokrzycki, V. Pashkkova, M. Ogura, J. Dedecek, Al-rich beta zeolites . Distribution of Al atoms in the framework and related protonic and metal-ion species, J. Catal. 333 (2016) 102–114. doi:10.1016/j.jcat.2015.10.010.

[30] J. Pérez Pariente, M. Sánchez-Sánchez, eds., Structure and Reactivity of Metals in Zeolite Materials, Springer International Publishing, Cham, 2018. doi:10.1007/978-3-319-98905-1.

[31] B. Rhimi, M. Mhamdi, V.N. Kalevaru, A. Martin, Synergy between vanadium and molybdenum in bimetallic ZSM-5 supported catalysts for ethylene ammoxidation, RSC Adv. 6 (2016) 65866–65878. doi:10.1039/C6RA09736G.

[32] B. Sulikowski, J. Klinowski, Dealumination of zeolites with silicon tetrachloride vapour. Part 6.-Zeolites Li, Na-X and Li, Na-Y, J. Chem. Soc. Faraday Trans. 86 (1990) 199–204. doi:10.1039/FT9908600199.

[33] F. Thibault-Starzyk, I. Stan, S. Abelló, A. Bonilla, K. Thomas, C. Fernandez, J.-P. Gilson, J. Pérez-Ramírez, Quantification of enhanced acid site accessibility in hierarchical zeolites – The accessibility index, J. Catal. 264 (2009) 11–14. doi:10.1016/j.jcat.2009.03.006.

[34] C. Freitas, N.S. Barrow, V. Zholobenko, Accessibility and Location of Acid Sites in Zeolites as Probed by Fourier Transform Infrared Spectroscopy and Magic Angle Spinning Nuclear Magnetic Resonance, Johnson Matthey Technol. Rev. 62 (2018) 279–290. doi:10.1595/205651318X696792.

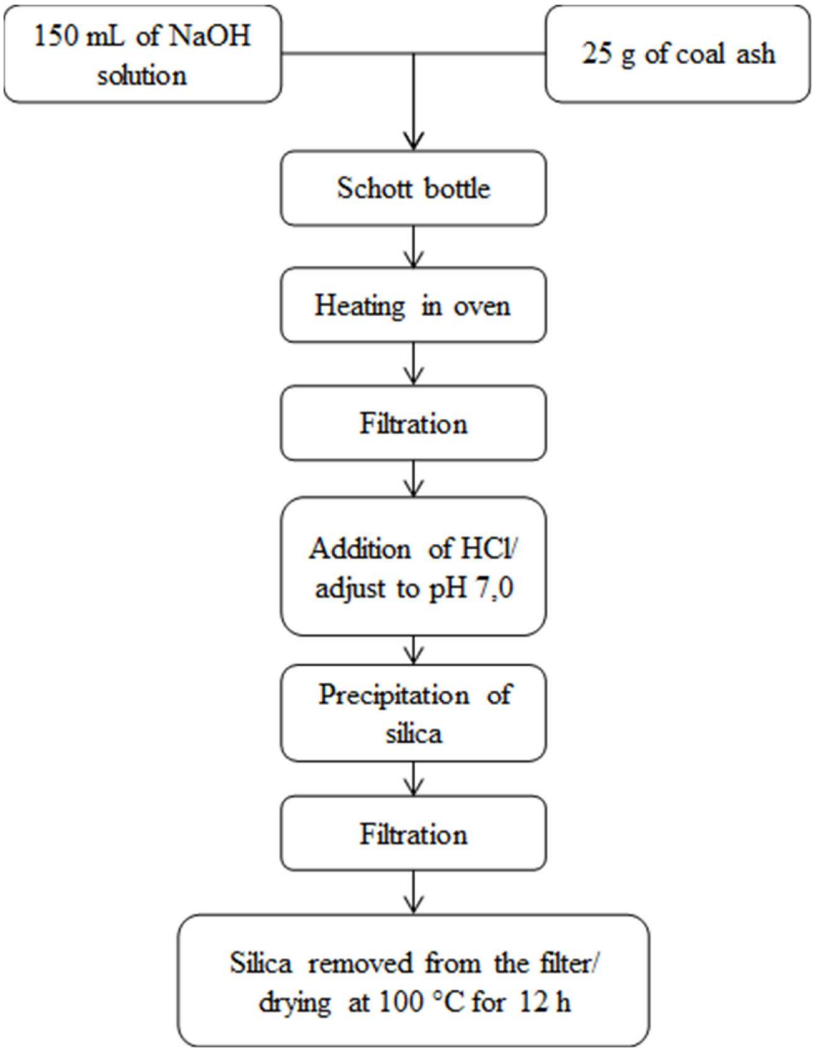

Figure 1. Schema of silica extraction from fly ash.

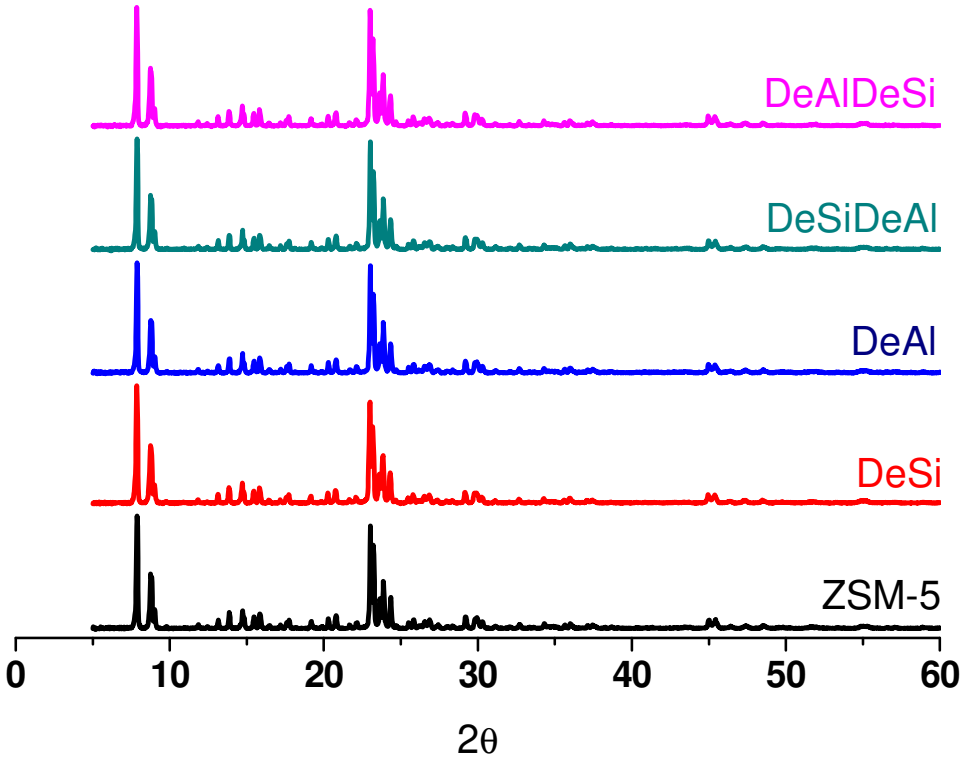

Figure 2. XRD patterns of the ZSM-5 zeolites

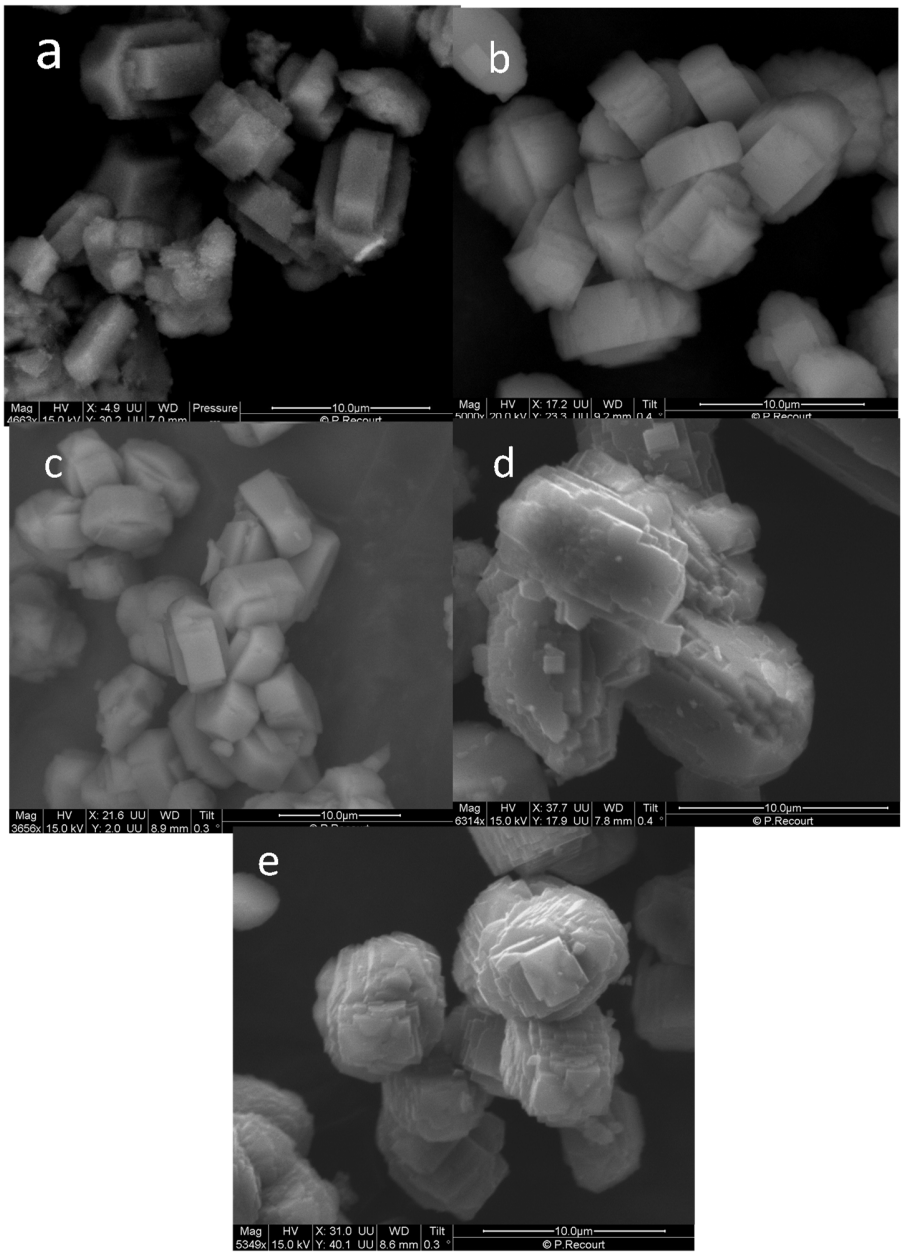

Figure 3. SEM images of the parent ZSM-5 zeolite (a), DeSi (b), DeAl (c), DeSiDeAl (d), DeAlDeSi (e)

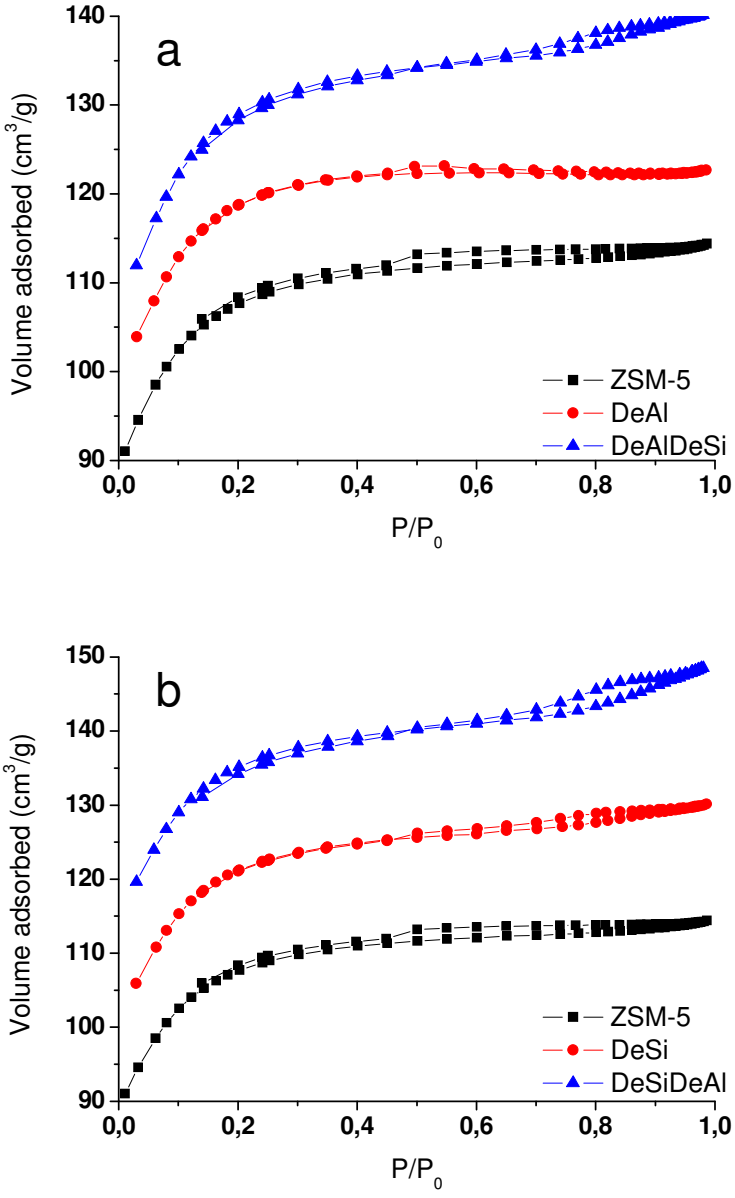

Figure 4. Isotherms of nitrogen adsorption-desorption over dealuminated and dealuminated-desilicated ZSM-5 (a), over desilicated and desilicated-dealuminated ZSM-5 (b).

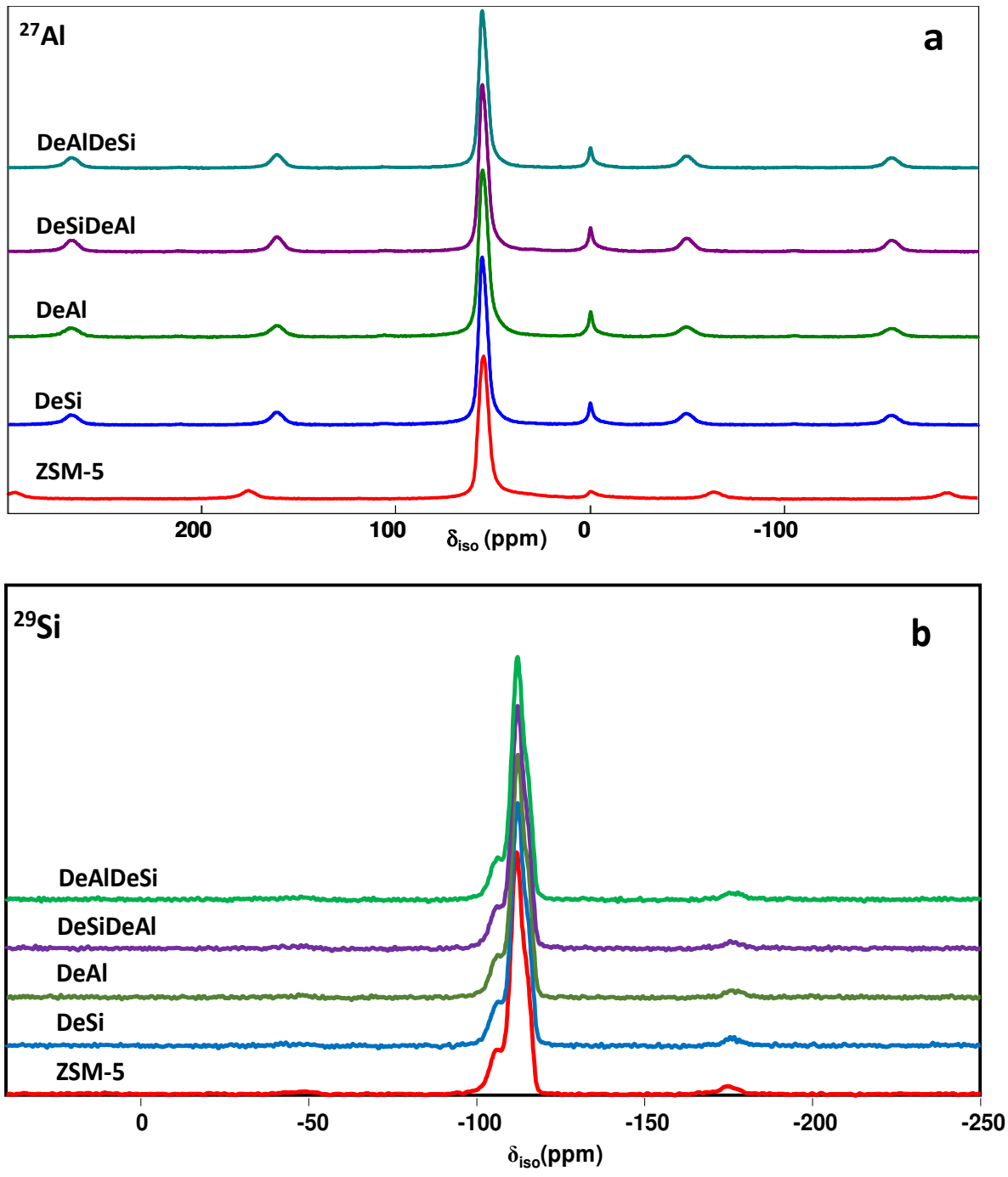

Figure 5. ^{27}Al MAS-NMR (a) and ^{29}Si MAS-NMR (b) spectra of ZSM-5 zeolites

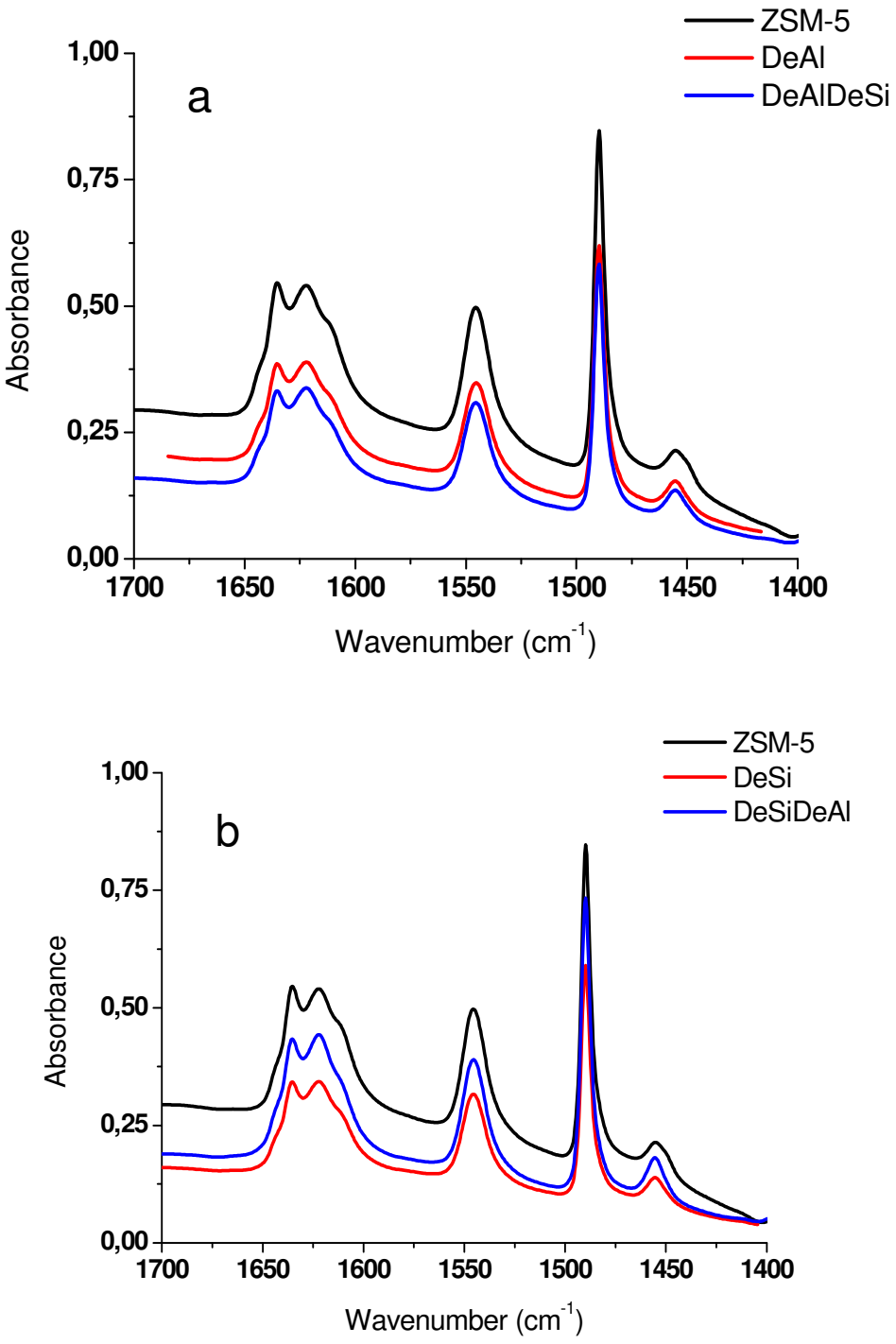

Figure 6. FTIR spectra of Py adsorbed on over dealuminated and dealuminated-desilicated - ZSM-5 (a), over desilicated and desilicated-dealuminated ZSM-5 (b)

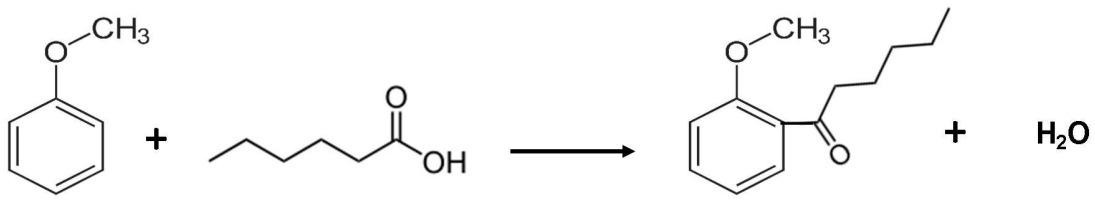

Figure 7. Acylation of anisole with hexanoic acid

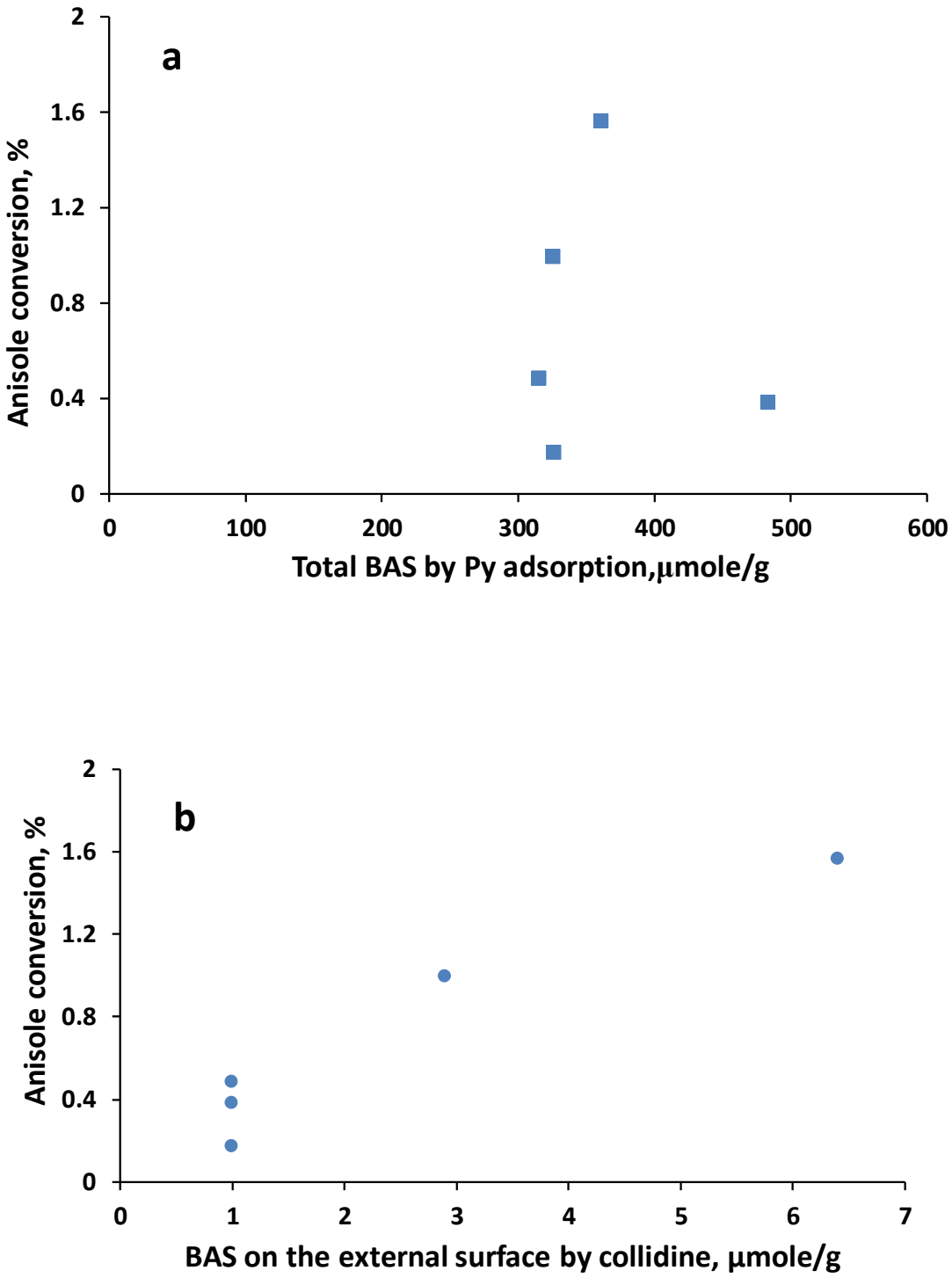

Figure 8. Anisole conversion over zeolites as a function of the total conversion of Bronsted acid sites measured by Py adsorption (a) and a concentration of Bronsted acid sites on the zeolite external surface (b).

Table 1. Textural properties and chemical composition of the ZSM-5 zeolites.

	S_{BET}[a] ($m^2.g^{-1}$)	S_{ext} ($m^2\ g^{-1}$)	V_{meso}[a] ($cm^3.g^{-1}$)	V_{micro}[a] ($cm^3.g^{-1}$)	Si/Al from XRF
ZSM5	460	109	0.067	0.133	17.0
DeSi	453	125	0.068	0.132	14.5
DeAl	443	124	0.060	0.129	14.2
DeSiDeAl	448	130	0.077	0.129	15.1
DeAlDeSi	480	143	0.080	0.137	14.6

Table 2. Fractions of aluminum atoms in different coordinations from ^{27}Al MAS NMR.

	Al^{IV}	Al^{V}	Al^{VI}
	56 ppm	28 ppm	0 ppm
ZSM-5	82	9	9
DeSi	92		8
DeAl	92		8
DeSiDeAl	91		9
DeAlDeSi	93		7

Table 3. Integrated intensity (%) of the ^{29}Si MAS-NMR peaks relating Si(nAl) building units and Si/Al ratio calcuted from ^{29}Si MAS-NMR.

	Si(1Al)	Si(0Al)	Si(0Al)	Si/Al ratio
	-106.2 ppm	-111.9 ppm	-115.3 ppm	
ZSM5	21	63	16	19
DeSi	20	63	17	20
DeAl	20	62	18	20
DeSiDeAl	20	63	17	20
DeAlDeSi	19	64	17	21

Table 4. Concentration of Bronsted and Lewis acid sites in the ZSM-5 zeolites.

	Number of acid sites, μmol.g^{-1}		
	Pyridine		Collidine
	Brønsted[a]	Lewis[a]	Brønsted[b]
ZSM5	483	50	1
DeSi	332	40	3
DeAl	335	39	1
DeSiDeAl	363	51	6
DeAlDeSi	310	40	1

[a] obtained by IR spectroscopy with pyridine adsorption at 150°C

[b] obtained by IR spectroscopy with collidine adsorption at 150°C

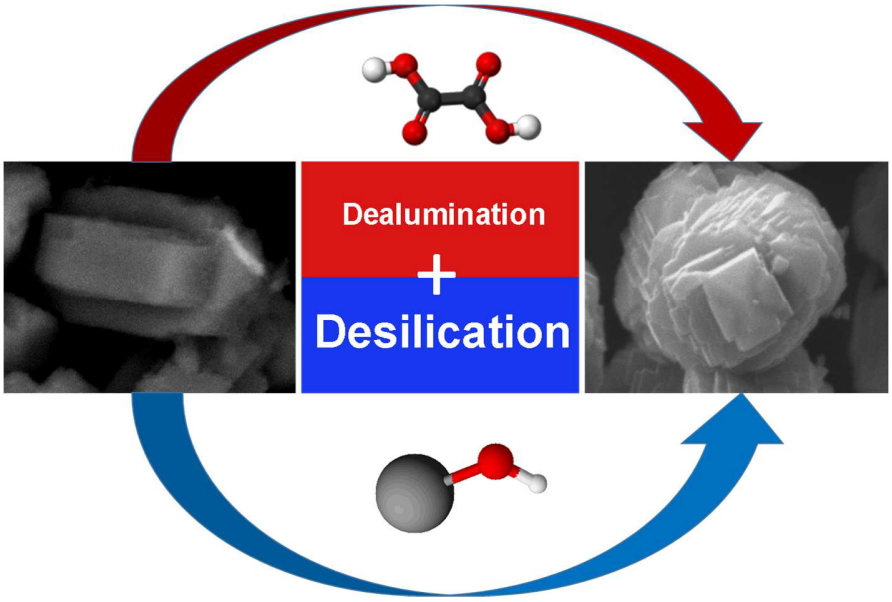
Dealumination
+
Desilication